Journal of Power Sources 195 (2010) 8280–8288

Contents lists available at ScienceDirect

Journal of Power Sources

journal homepage: www.elsevier.com/locate/jpowsour

$LiFePO_4$: From molten ingot to nanoparticles with high-rate performance in Li-ion batteries

K. Zaghib[a,*], P. Charest[a], M. Dontigny[a], A. Guerfi[a], M. Lagacé[a], A. Mauger[b], M. Kopec[c], C.M. Julien[c]

[a] Institut de Recherche d'Hydro-Québec, 1800 Lionel Boulet, Varennes, QC, Canada J3X 1S1
[b] Université Paris 06, IMPMC, 140 rue de Lourmel, 75015 Paris, France
[c] Université Paris 06, INSP, 140 rue de Lourmel, 75015 Paris, France

ARTICLE INFO

Article history:
Received 7 May 2010
Received in revised form 5 July 2010
Accepted 6 July 2010
Available online 23 July 2010

Keywords:
Li-ion batteries
Positive electrode
Olivine
Nanoparticles
Molten state

ABSTRACT

$LiFePO_4$ (LFP) particles were obtained by grinding ingot synthesized in the molten state. This process, followed by jet milling, and then wet milling, provides a simple way to obtain powders with controlled particle size in the range from macroscopic to 25 nm. However, at this time, we find that these particles tend to agglomerate to form secondary particles of size ~100 nm. The particles obtained by this process are characterized by X-ray diffraction (XRD). In situ and ex situ scanning electron microscopy (SEM) and transmission electron microscopy (TEM). The effect of milling was also investigated by analysis of physical properties using infrared spectroscopy (FTIR) and magnetic measurements. The electrochemical performance was evaluated in cells containing Li/1 M $LiPF_6$ in EC:DEC (1:1)/C-$LiFePO_4$. After carbon coating, the LFP particles which are free of impurities, exhibit high-rate capability. Even with a limited amount of carbon (2 wt.%) appropriate for commercial batteries, the capacity is 157 mAh g^{-1} at 0.1 C, 120 mAh g^{-1} at 10 C, without capacity fading after 60 cycles.

1. Introduction

Following the pioneering work of Padhi et al. [1,2], $LiFePO_4$ (LFP) has been extensively studied owing to its use as the active cathode element in a new-generation of lithium-ion batteries. This success is due to its environmental compatibility, thermal stability, and long cycling life (for a review, see Ref. [3]). The LFP particles have very small electronic conductivity, but it is a common practice in the production of Li-ion battery cathodes to add carbon either to the $LiFePO_4$ matrix [2,4] or by surface coating the $LiFePO_4$ particles with thin layers of carbon [5–7]. The carbon formed by a spray pyrolysis technique increases the electronic conductivity by seven-order-of-magnitude [7]. As a result, a capacity of about 160 mAh g^{-1}, which close to the theoretical value, was obtained with $LiFePO_4$ coated with ca. 2 wt.% carbon [5]. In addition, the redox potential is ca. 2.5–4.0 V vs. Li^+/Li^0, which is the potential window required with the common electrolytes.

Many synthesis routes have been adopted to synthesize $LiFePO_4$ involving solid-state reactions [8–11], sol–gel [12,13], hydrothermal [14–17], co-precipitation [18,19], polyol process [20], microemulsion [21], spray [22,23], microwave synthesis [17,24,25], template method [26–28], solvothermal method [29,30], or reverse micelle process [31]. Currently, most processes produce $LiFePO_4$ powder with capacity close to theoretical, provided the synthesis is performed under reducing atmosphere to avoid oxidation of iron inform the Fe^{3+}-based impurity phases [32]. However, another parameter greatly influences the rate capability, namely the particle size, because of the short diffusion length for Li^+ ions [33,34]. Applications in portable electronic devices do not necessarily require a lot of power, but power is important for electric vehicles. Thus, extensive effort has been devoted to reduce the particle size [35–37], nevertheless, too small particles reduce the tap density [38]. It is then important to monitor the size of the particles so that it is optimized to the desired value, depending on the targeted application. For this purpose, synthesis of $LiFePO_4$ in the molten state has been proposed recently [39].

The aim of this present work is to prepare nano-sized LFP particles from ingot obtained by molten-state synthesis (Fig. 1). We show that the process is fast and simple, and offers the desired flexibility to control the size of the particles. We also observed that the process produces LFP particles that are free of impurities. In addition, another advantage of this preparation process is that more spherical shape particles are obtained. The Li^+ ions preferably move along the *b*-axis of the crystal with orthorhombic space group *Pnma* [40,41]. It is then desirable to reduce the crystallite size along this axis. However, this is a difficult problem because there is a tendency of the particles to grow in the form of plates in the (*ab*) plane [42,43], although the thickness along the *b*-axis is reduced to

* Corresponding author. Tel.: +1 450 652 8019; fax: +1 450 652 8424.
E-mail address: Zaghib.karim@ireq.ca (K. Zaghib).

0378-7753/$ – see front matter © 2010 Elsevier B.V. All rights reserved.
doi:10.1016/j.jpowsour.2010.07.010

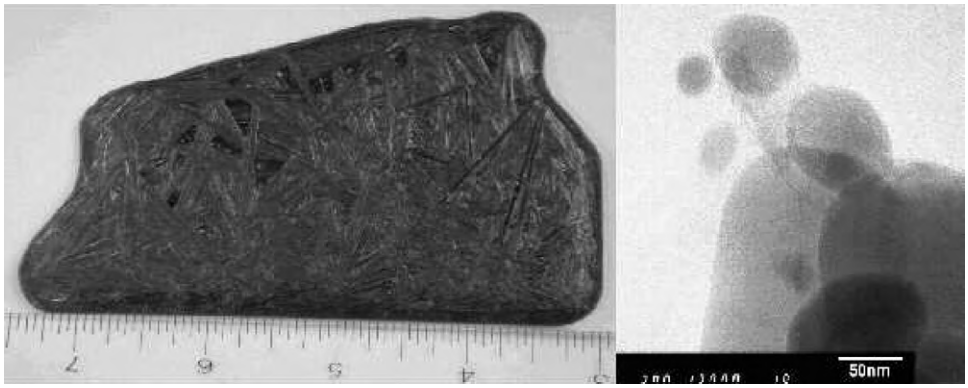

Fig. 1. Left: Picture of the LFP molten ingot; scale is in cm. Right: TEM image of nano-LFP after wet milling and carbon coating.

30–40 nm in some cases [29,44–46]. For some synthesis routes, the reduction to small size occurs at the expense of crystallinity and the formation of a large concentration of defects [45] that reduces the electrochemical performance. Small crystallized particles can be achieved by solvothermal method [29] and also by milling process [47]; it is this second route that is explored in this work. The electrochemical performance of the LFP nanoparticles in positive electrodes were tested in cells using 2 wt.% carbon only. Still, the rate capability for the C-$LiFePO_4$ nanoparticles in Li/1 M $LiPF_6$ in EC:DEC (1:1)/C-$LiFePO_4$ cells is remarkable.

2. Experimental

2.1. Synthetic procedure

In the first step, $LiFePO_4$ was synthesized by the procedure described in [48], i.e. a solid-state reaction of $FePO_4{\cdot}2H_2O$ and Li_2CO_3 mixed at nominal composition for $LiFePO_4$ (i.e. in the ratio 2:1) to avoid the formation of local defect (iron on Li site) in case of Li deficiency, or Li_3PO_4 impurity phase in case of excess of lithium [49]. An excess of 0.5 mole fraction of EBN-1010 (graphite powder) was added to the initial product as a reducing agent for iron by adding the polymer. Then, the mixture was heated to 1050 °C for 5 min in a graphite crucible and then cooled under Ar or N_2. The ingot typically obtained by this process is illustrated in Fig. 2. Low cost precursors as iron metal (Fe), LiOH and H_3PO_4 are used to prepare ingot.The second step is to break the ingot to produce small particles. At this stage, the ingot is too large for a roll crusher. Therefore, it was first crushed into centimeter-size particles by using a jaw-crusher with ceramic liner to avoid metal contamination. Only then was the roll crusher (ceramic type) used to obtain millimeter-size particles. The millimeter-size particles are further ground by jet-mill to achieve micrometer-size particles. In the process, the grains enter the grading wheel and are blasted to cyclone separator and collector. The optimized particles are in the collector, while the larger ones are in the cyclone separator. For completeness, both have been studied in the present work, and the labels "collector" and "cyclone" will identify them. The smallest size that can be reached by this process is in the order of a micrometer. To obtain smaller particles, the micrometer-size powders were dispersed in isopropyl alcohol (IPA) solution at 10–15% of solid concentration and then ground on a bead mill using 0.2-mm zirconia beads to obtain nanometer-size particles. This wet-milling process is described in Ref. [50].

At this stage, the particles are carbon-free. The third step involved the following procedure to obtain carbon-coated particles. The particles were mixed with the carbon precursor (lactose) in acetone solution. The nominal dry additive corresponded to 5 wt.% carbon in $LiFePO_4$. After drying, the blend was heated at 700 °C for 4 h in an inert atmosphere. The final quantity of carbon was about 2 wt.% of the material (C-detector, LECO Co., CS 444). During this process, the organic precursor for the carbon acts as a reducing agent [51]. The flowchart of the whole process is shown in Fig. 2.

2.2. Structural and physical characterization

The crystal structure of the particles was analyzed by X-ray diffraction (XRD) with a Philips X'Pert apparatus equipped with a Cu Kα X-ray source (λ = 1.5406 Å) and a Bruker AXS D8 ADVANCE with Bragg-Brentano geometry, which has a sealed Co Kα radiation source (including both Kα1 and Kα2) and linear 1-D position sensitive detector (Vantec-1), where Kβ radiation is filtered by Fe foil. XRD measurements were collected in the 2θ range 10–80° in step scanning mode $\Delta(2\theta) = 0.05°$. The structural parameters

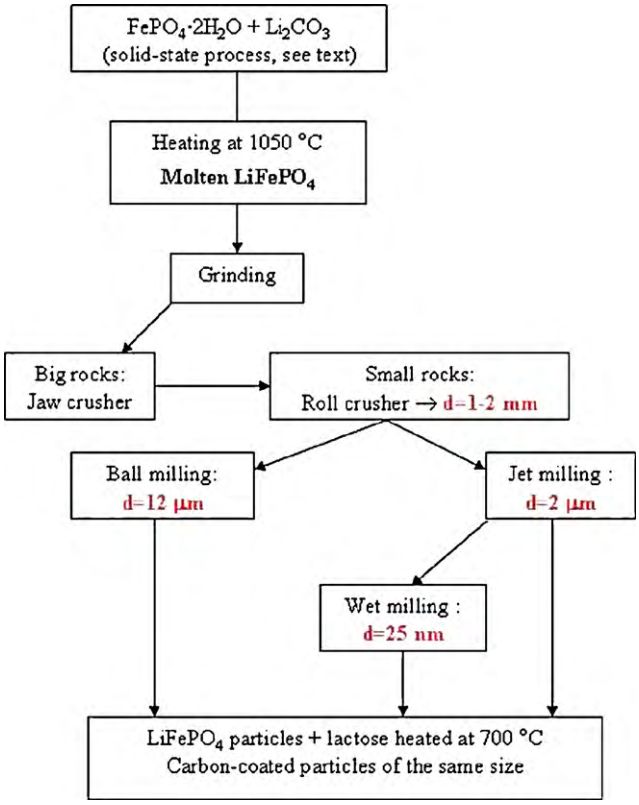

Fig. 2. Flowchart for preparation of $LiFePO_4$ powders by synthesis in the molten state. *d* is the mean size of the primary particles obtained at different steps in the process and measured by analysis of SEM images.

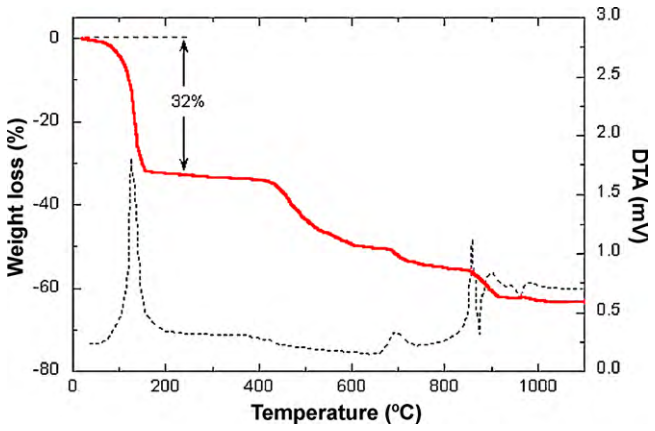

Fig. 3. TG-DTA of samples with two endotherms corresponding to evaporation of water and loss of structural water. The melting temperature of $LiFePO_4$ is associated with the peak at 950 °C.

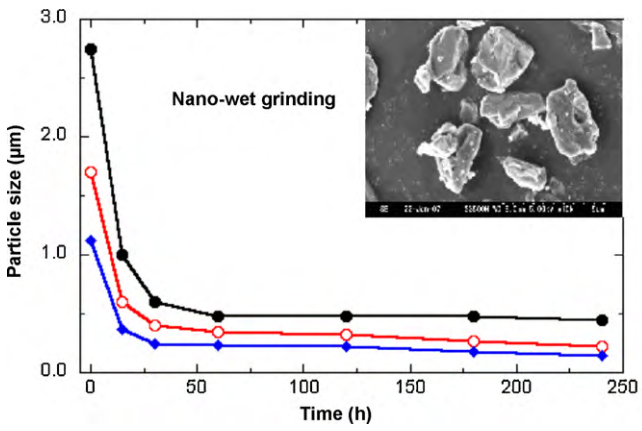

Fig. 4. Secondary particle size as a function of wet-milling time for three different samples taken at different steps of the roll milling process, i.e. with three different mean size of particles at $t = 0$. Inset is SEM image of the sample with the largest particle size (2.8 μm) before jet milling. Note that, before jet milling, there is no agglomerate so that the notion of primary and secondary particles is meaningless. Upon jet milling, however, the secondary particles, which is measured by diffusion of a laser beam, are agglomerates of thinner particles observed by electron microscopy analysis.

were determined by Rietveld refinement of the diffraction profiles. Scanning electron microscopy (SEM) and transmission electron microscopy (TEM) images were obtained using an electronic microscope Hitachi model HD-2700 with 200 kV, 120 kV and 80 kV operating potential. The TEM samples were ultrasonically treated in a solution of isopropyl alcohol and then deposited on silica substrate.

The thermal decomposition of the gel precursors was examined by differential thermal analysis (DTA) using a Netzsch analyser (model STA 409). Experiments were carried out in an ambient atmosphere with a heating rate of 0.1 °C s^{-1}.

The particle size was measured by a high-performance laser diffraction analyzer. The LA-950V2 uses Mie scattering (laser diffraction) to measure particle size of suspensions or dry powders. The speed and ease-of-use of this technique makes it the most popular for many applications.

FTIR absorption spectra were recorded with a Fourier transform interferometer (model Bruker IFS113v) in the wavenumber range 150–1400 cm^{-1} at a spectral resolution of 1 cm^{-1}. Magnetic measurements (susceptibility and magnetization) were carried out with a fully automated magnetometer (MPMS-5S from Quantum Design) with a superconducting quantum interference device (SQUID) in the temperature range 4–300 K.

2.3. Electrochemical studies

The electrochemical experiments were carried out in cells with metallic lithium as the negative electrode using the coffee-bag technology developed at Hydro-Quebec. The coffee-bag or laminated battery technology was described elsewhere [9]. The electrolyte was 1 M $LiPF_6$ in EC:DEC (1:1) solvent [EC = ethylene carbonate, DEC = diethylene carbonate (LP40-Merk)]. The cell was charged and discharged at C/10. All the electrochemical properties reported here were measured at room temperature.

3. Results

3.1. Thermal analysis

The exact temperature of the phase formation reaction of the $LiFePO_4$ olivine was studied using thermogravimetric analysis (TG/DTA) on the precursor complex $FePO_4 \cdot 2H_2O$ and Li_2CO_3 mixed at nominal composition. Fig. 3 shows the thermogram of $LiFePO_4$ in the range from 30 to 1100 °C. These results display several discrete weight-loss regions with distinguishable transformation enthalpies. The first endothermic peak observed at about ca. 120–150 °C is accompanied by a noticeable weight loss (~32%) in the TG curve. This is attributed to the superficial water loss due to the hygroscopic nature of the iron phosphate. As the process of heating continues, two significant weight losses occur at ca. 400 °C due to the departure of CO_2 from Li_2CO_3 decomposition and then a carbothermal reduction of Fe^{3+} at ca. 700 °C. Finally, the melting endothermal peak was observed at 965 °C.

The choice of 700 °C for the final heat treatment of LFP particles results from a compromise, since the carbon film is more conductive when heating at higher temperatures [52]. However, heating at higher temperature runs the risk of increasing diffusion between particles of agglomerates, in which case the size of the primary particles change and leads not only to carbon coating, but also in a modification of the topology of the primary particles. The topology might be masked by the carbon layer that covers the secondary particles. To explore this effect, we examined in situ SEM images of $LiFePO_4$ (before carbon coating) as a function of temperature up to the melting point. No change of the topology was observed up to 700 °C. However, we observed such effects at $T \geq 750$ °C. That is why we restricted the heating process to 700 °C only. On one hand, it is low enough to make sure that the particle size and topology are not modified in the process. On the other hand, we know from earlier work [52] that this temperature is sufficient to guarantee that the variety of carbon deposited on the $LiFePO_4$ is coke that is conductive.

3.2. Structural properties

The smallest LFP particles were obtained by wet-milling process. Fig. 4 shows the size of the secondary particles as determined by laser spectroscopy as a function of the wet-milling time. The reduction in particle size occurs rapidly in the first 15 min of the milling process, then its deceases gradually to100 nm after 2 h.

The XRD pattern for the final powder is shown in Fig. 5, together with the XRD pattern of 2-μm particles for comparison. In both cases, all the diffraction peaks are identified as those of the $LiFePO_4$ with the space group *Pnma*, and no impurity phase is detected. The lattice parameters are $a = 10.331(3)$ Å, $b = 6.010(1)$ Å, $c = 4.693(2)$ Å, with a unit cell volume $V = 291.3(8)$ $Å^3$. These data are in agreement with those found in the literature [1,47,30]. In particular, the volume of the unit cell is characteristics of the samples that are free from stoichiometric defects [49]. The large broadening of the

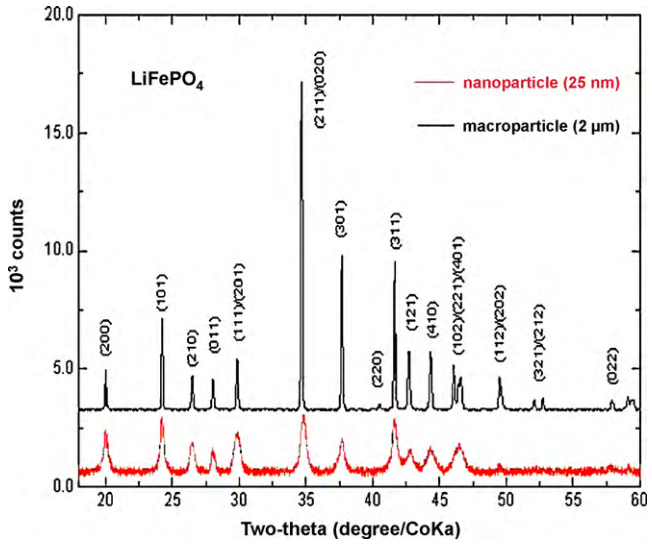

Fig. 5. XRD pattern of sample with 25-nm primary particles and 100-nm secondary particles (lower spectrum) obtained after jet milling (in red). The XRD pattern for a sample with particle size 2 μm (upper spectrum) is also reported for comparison (in black). (For interpretation of the references to color in this figure legend, the reader is referred to the web version of the article.)

XRD lines of the nano-sized particles implies that the instrumental broadening is negligible, and the coherence length for the sample with the nano-sized particles l can be deduced from the Scherrer law $l = k\lambda/(B\cos\theta)$ with B the half-width of the diffraction peaks, λ the wavelength of the X-ray beam and $k = 0.9$. The result is $l = 25$ nm.

The SEM image of the sample before wet milling (micron-size particles) is shown in Fig. 4, while the image after wet milling is shown in Fig. 6. The size d of the primary particles is about 25 nm, smaller than the size (≈100 nm) of the secondary particles determined by laser, but in agreement with the coherence length determined from XRD. These results suggest that the primary particles are crystallites. Therefore, the sample obtained by wet milling is a powder with single-crystalline primary particles of typical size $d = 25$ nm, with a low fraction of agglomeration to form secondary particles of typical size 100 nm.

TEM images of this sample are shown in Fig. 7, before and after carbon coating. They show the same features. In addition, we find the carbon layer is homogeneous. From now on, we report the properties of three samples that we identify in this work by the milling stage (roll, jet, wet mill) or by the size d of their particles: $d = 2$ mm, 2 μm, 25 nm, respectively.

3.3. FTIR analysis

The FTIR probes the structure of $LiFePO_4$ at the molecular scale, accessing the vibration modes of the ions, primarily associated to the motion of iron and phosphate. The spectra of the samples obtained immediately following roll, jet and wet milling are presented in Fig. 8. Since the carbon absorbs light, it is not possible to measure the FTIR spectra of the carbon-coated samples. On the other hand, we measured the FTIR spectra of the jet-milled samples after the same heating treatment (at 700 °C for 4 h under reducing atmosphere) that is used in the carbon-coating process, but without the carbon precursor. This experiment showed the effect of heat treatment on the particles. The results are shown in Fig. 9. The posi-

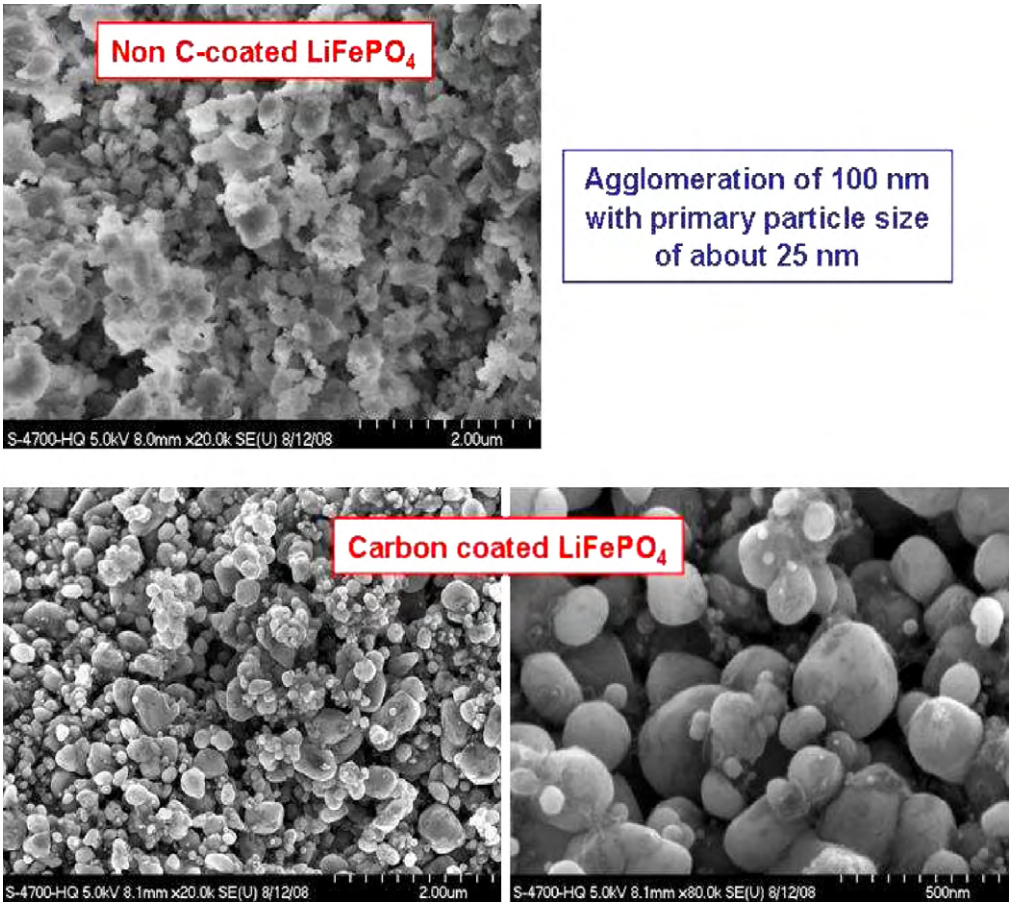

Fig. 6. SEM images of sample with 100-nm secondary particles obtained from primary particles with $d = 25$ nm.

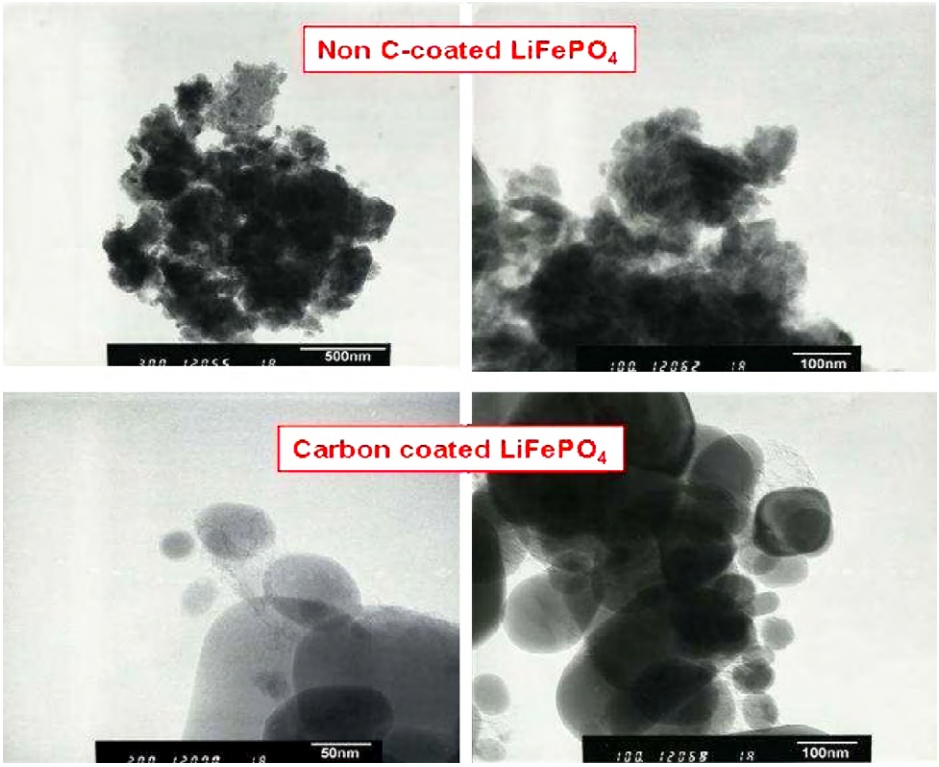

Fig. 7. TEM images of the sample with 100-nm secondary particles obtained from primary particles with $d = 25$ nm.

tions of the intrinsic bands in the spectra of $LiFePO_4$ are well known [53], and are also evident in Fig. 9. The first result is that all the bands that we observe in Figs. 8 and 9 are intrinsic in nature. The bands in the range 372–647 cm^{-1} are bending modes (ν_2 and ν_4) involving $(PO_4)^{3-}$ symmetric and asymmetric modes and Li vibrations. The bands in this spectral range are thus sensitive to the local environment of the Li ions. Note this part of the spectrum is not affected by the carbon coating, which confirms that the carbon does not penetrate into the particles [3]. The part of the spectrum in the range 945–1139 cm^{-1} corresponds to the stretching modes of the $(PO_4)^{3-}$ units. They involve symmetric and asymmetric modes of the P–O bonds at frequencies closely related to those of the free molecule.

Other information that is derived from these spectra is that the absence of any band between 647 and 945 cm^{-1}. Since the vibration characteristic of the P–O–P bridging of P_2O_7 unit is right in the middle of this range, FTIR is quite a sensitive tool to detect any pyrophosphate impurity. Therefore, the lack of any structure in this frequency range is evidence that there are no $LiFeP_2O_7$ impurities in our samples. For the same reason, we do not have Li_3PO_4 impurities because the FTIR band at 430 cm^{-1} (see for instance [49]) that is attributed to impurities is not observed either. This is actually expected since the precursors have been mixed at nominal composition for $LiFePO_4$.

We also notice a broadening of the bands in the spectra in Fig. 8 as d increases: the most resolved spectra are observed in the wet-

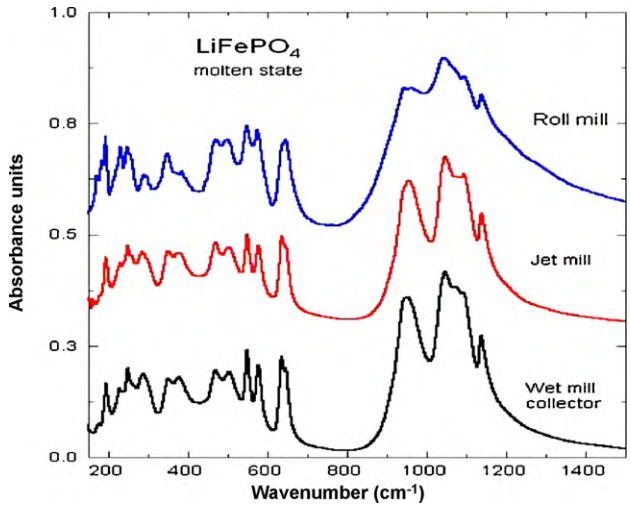

Fig. 8. FTIR absorption spectra of molten-state samples at different stages of the grinding process (before carbon coating).

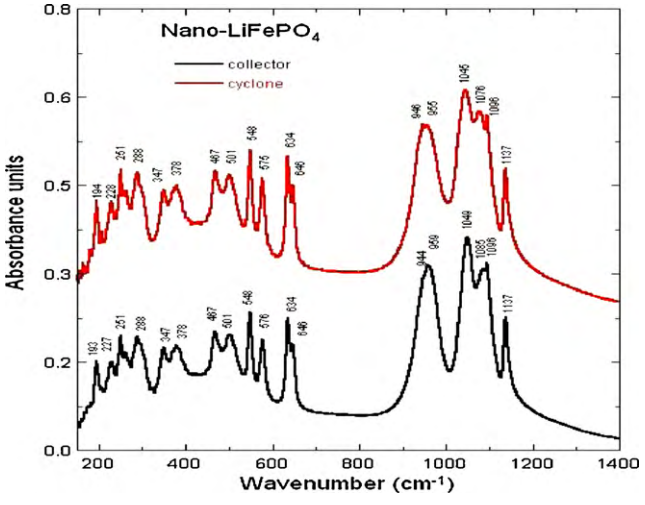

Fig. 9. FTIR spectra of jet-milled LFP obtained from the collector and the cyclone area (see text) after heating at 700 °C for 4 h, and before coating with carbon. The bands are identified as intrinsic vibration modes of $LiFePO_4$.

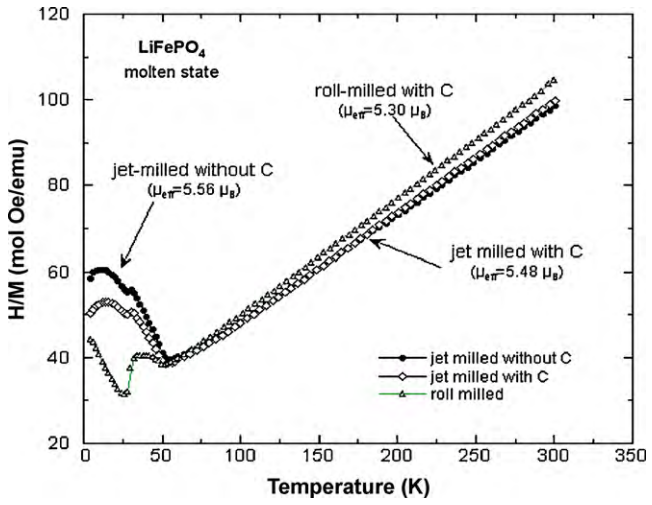

Fig. 10. Inverse of the magnetic susceptibility M/H measured in field $H = 10$ kOe, for roll and jet-milled samples before and after carbon coating, prepared from the ingot cooled in the molten state under argon atmosphere. Note the jump near 30 K, which is the signature of $Li_3Fe_2(PO_4)_3$ impurity.

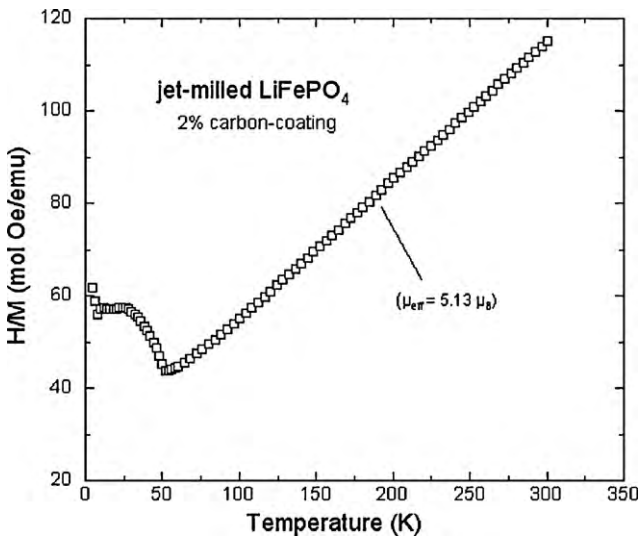

Fig. 11. Inverse of the magnetic susceptibility M/H measured in field $H = 10$ kOe, for jet-milled sample prepared from the ingot cooled in the molten state under N_2 + residual hydrogen atmosphere after carbon coating.

milled case. The broadening is the signature for a shorter lifetime of the vibration modes due to solid friction associated to defects [54]. The more resolved spectrum observed for smaller values of d is then attributable to the fact that smaller particles have less structural defects such as grain boundaries in the vicinity of the lattice that is less ordered (in the limit of nanoparticles $d = 25$ nm, the particles are also crystallites, $d \approx l$, and thus without any structural defect in the bulk of the particles). The only disorder for such small particles is located in the surface layer [47]. The data in Fig. 9 show that after heat treatment, the bands are even more resolved. This result shows that heat treatment at 700 °C induced a re-crystallization of the disordered surface layer. The surface/volume ratio is not negligible for such small particles, thus re-crystallization of the surface layer has an impact on the FTIR spectra, well evident in Fig. 9.

3.4. Magnetic properties

The most sensitive means of characterization for the material is investigation of the magnetic properties because $LiFePO_4$ is an antiferromagnet while most of the impurities that may be poisons are ferro- or ferri-magnetic components. We show in Fig. 10 the temperature dependence of the magnetic susceptibility $\chi = M/H$, with M the magnetization measured at $H = 10$ kOe, for jet-milled samples before and after carbon coating obtained from the molten state in argon atmosphere. $\chi(T)$ goes through a maximum at the Néel temperature $T_N = 50$ K. The magnetization curves of all the samples before (and after) carbon coating are linear in the range $H < 30$ kOe in the paramagnetic regime. We can then conclude that the samples are free from Fe_2O_3 and Fe_2P impurities, since a deviation of the magnetization curves is detected as soon as 0.1 at.% of iron is involved in the formation of such impurities. At $T = 30$ K, however, an anomalous jump of $\chi(T)$ is observed, which is linked to the onset of a spontaneous magnetization. This feature is the signature of the presence of NASICON impurity, as $Li_3Fe_2(PO_4)_3$ undergoes a first-order ferromagnetic order at this temperature. Note this impurity is not eliminated by the carbon-coating process, despite the reducing atmosphere during heating at 700 °C, which gives evidence that the NASICON impurities are not entirely localized at the surface. This is expected since an even larger quantity of $Li_3Fe_2(PO_4)_3$ is observed in the particles obtained after roll milling that are so big that surface effects are negligible. This impurity is formed during the synthesis of the molten ingot, and shows the necessity to prepare the molten ingot in a reducing atmosphere. The $Li_3Fe_2(PO_4)_3$ impurity is not observed when the synthesis is carried out in N_2 + residual hydrogen atmosphere. Fig. 11 shows the $\chi(T)$ curves for the jet-milled particles obtained from an ingot prepared in such a reducing atmosphere. The jump in $\chi(T)$ at 30 K has now disappeared, so these samples are free of NASICON impurity. Note that milling at any stage (crush, roll, jet, wet) is done in air, and does not lead to any pollution because it is performed at room temperature, too low to allow for nucleation of impurities.

The effective magnetic moment as deduced from the linear fit of the $\chi^{-1}(T)$ is larger than the theoretical value 4.92 μ_B for Fe^{2+} in the high-spin state for the samples in Fig. 10. This is again the spurious effect of the NASICON impurity. However, for the jet-milled sample in Fig. 11, the effective magnetic moment is reduced to 5.13 μ_B. This is further evidence that this sample is free of any impurity, the small difference with respect to the theoretical value being reduced to the magnetic polaron effect [3].

3.5. Electrochemical properties

The electrochemical performance of jet-milled C-$LiFePO_4$ (prepared in N_2 plus residual hydrogen) is shown in Fig. 12. The results match the performance of the best samples reported in many prior works. The reversible capacity is 157 mAh g^{-1}; the voltage as a function of the lithiation/delithiation rate has a plateau at 3.4 V, characteristics of the phase separation between Li-rich and Li-poor phases in well-crystallized samples.

The results in the published literature on electrochemical properties of nanoparticles are much more diverse, and even controversial because some authors have claimed that there is no need for a carbon coating on particles of the typical size obtained by wet milling [18,55]. We believe that this conclusion is erroneous. The reason is linked to the fact that the surface to volume ratio is very important in such small particles, and the electrochemical performance of these particles depends very much on the surface layer. To clarify this situation, we have investigated the properties of the wet-milled particles at three different steps: (i) particles after jet milling without any treatment, (ii) particles heated at 700 °C for 4 h, but without any carbon additive, just to explore the effect of the heating treatment, and (iii) carbon-coated particles that have undergone the same thermal treatment (700 °C for 4 h with the carbon additive). The comparison between the two last cases will

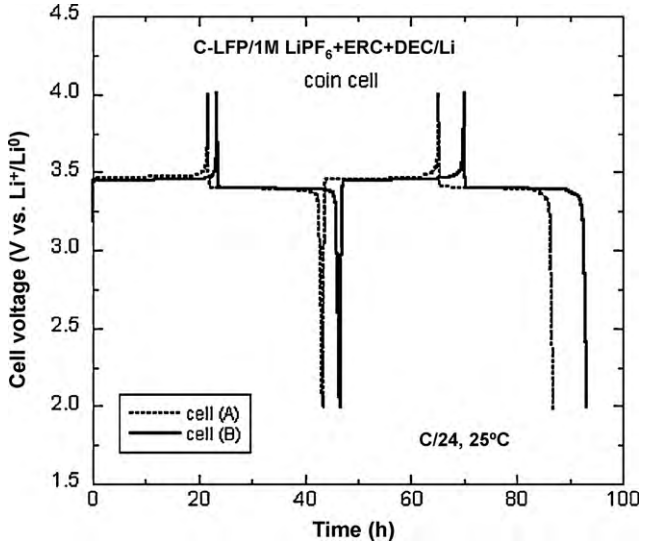

Fig. 12. Charge–discharge plot for two cells jet-milled C-$LiFePO_4$/1 M $LiPF_6$ + EC:DEC (1:1)/Li at C/24 rate. The $LiFePO_4$ used for the cathode has been obtained form the ingot cooled under nitrogen + residual hydrogen atmosphere and has been collected from the collector (cell A) and the cyclone area (cell B).

allow separation between effects due to the thermal treatment and the effect of the carbon deposit.

The charge–discharge curves in Fig. 13 show that the powder without any thermal treatment has very poor electrochemical properties, which was expected because the surface layer in that case is strongly disordered over a thickness of about 3 nm [47]. The performance is better with the powder that was heated at 700 °C without a carbon coating. Yet, Fig. 14 shows only 2% of the theoretical capacity is available during the first charge and the reversible capacity is only 8%. The improvement after heat treatment is evidence that the disorder of the surface layer was partially eliminated. Nevertheless, the electrochemical performance expected for $LiFePO_4$ is obtained only by carbon coating, as shown in Fig. 15. This figure shows the charge–discharge cycle for a sample

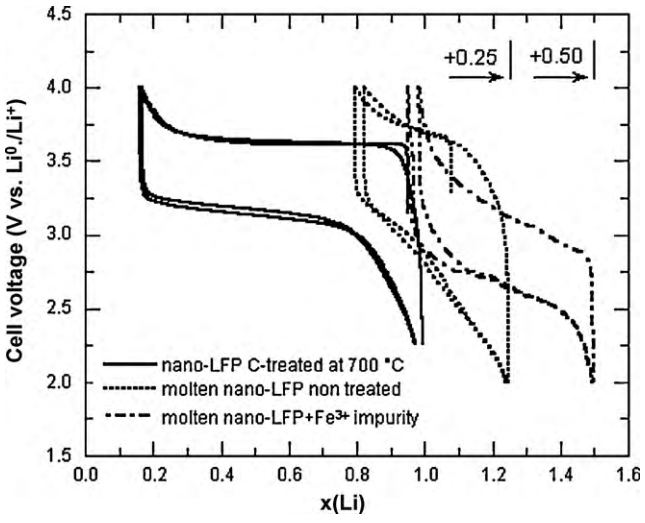

Fig. 13. Electrochemical performance at rate 0.1 C rate of cells prepared with wet-milled particles before any treatment, after heating at 700 °C for 4 h without carbon, and with carbon coat for comparison. The abscissa is the lithium concentration for the cell prepared with wet milled C-$LiFePO_4$ free of impurity, but is shifted by 0.25 to separate the plots. The result is also reported, shifted by 0.5, for a cell prepared with nanoparticles issued from the same ingot as in Fig. 10 including $Li_3Fe_2(PO_4)_3$ impurity, before carbon coating, to illustrate the dramatic effect of the Fe^{3+}-impurity.

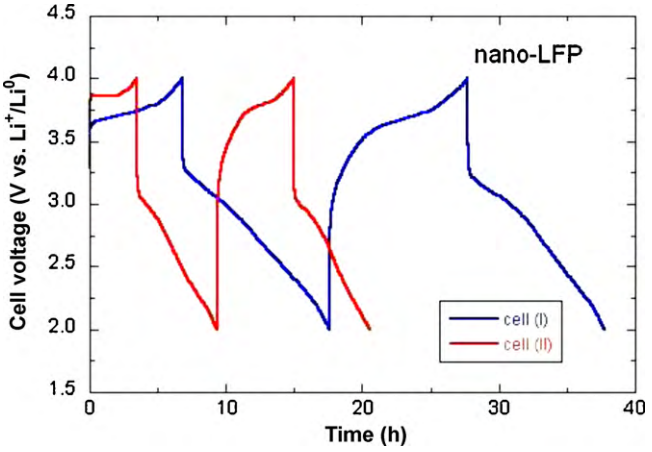

Fig. 14. Charge–discharge plot for wet-milled $LiFePO_4$ heated at 700 °C for 4 h without carbon coating. Measurements in cell with electrolyte 1 M $LiPF_6$ + EC:DEC (1:1) and Li counter electrode. Carbon coating is needed to enhance the electrochemical performance of Li cells. In cell I, the $LiFePO_4$ has been obtained from the ingot cooled in Ar atmosphere, while it has been extracted from the ingot cooled in N_2 plus residual hydrogen in cell II.

prepared in argon (i.e. poisoned with the NASICON impurity) and in N_2 + residual hydrogen (free from any impurity). It is clearly evident that the impurity has a detrimental affect on the electrochemical performance.

For the carbon-coated wet-milled particles prepared from the molten ingot in N_2 + residual hydrogen, the full capacity of 157 mAh g^{-1} is obtained at low rate (C/10). For comparison, the Ragone plots of the batteries prepared with the jet and wet-milled particles are presented in Fig. 16. The high-rate capability with wet milled particles is significantly higher than that for the jet-milled particles, as expected since the path length of Li^+ ions in the particles during the lithiation/delithiation process is less. No aging is observed during the first 60 cycles (see Fig. 17).

4. Discussion

The inert atmosphere (argon) did not prevent the formation of the $Li_3Fe_2(PO_4)_3$ impurity in the $LiFePO_4$ ingot that was prepared in the molten state. This is one of the most common impurities that can poison LFP because it is the natural iron phosphate in which iron is trivalent. However, preparation in N_2 that contains a small

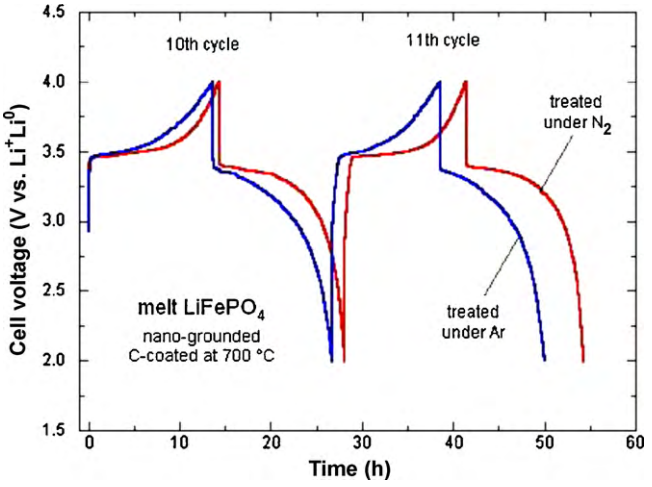

Fig. 15. Charge–discharge of the cell prepared with wet-milled powder after carbon coating and heat treatment under Ar and N_2 atmosphere.

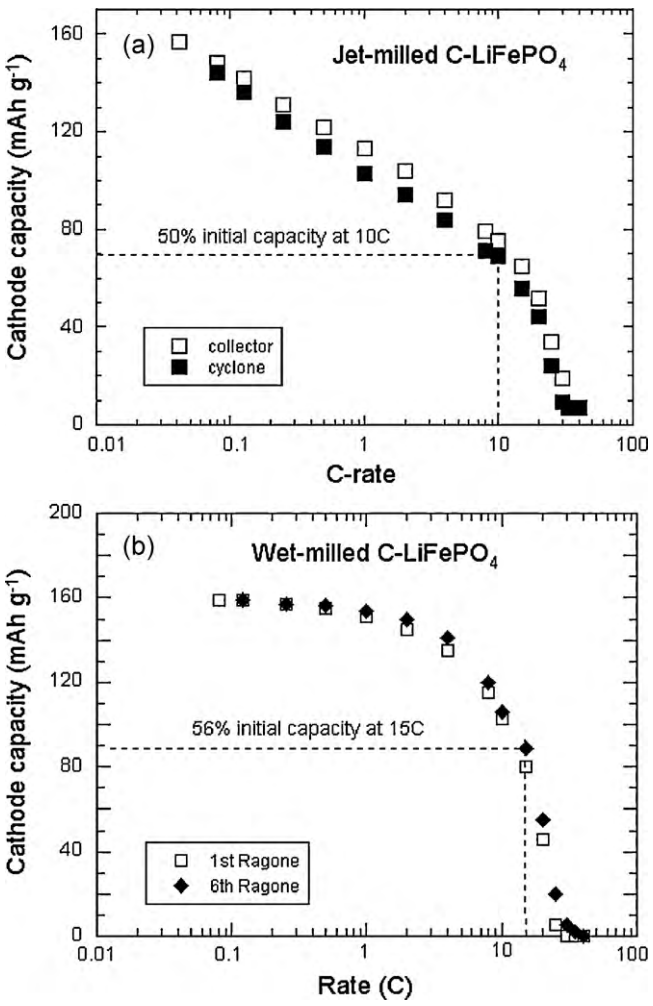

Fig. 16. Ragone plot for jet-milled (a) and wet-milled (b) C-$LiFePO_4$/1 M $LiPF_6$ + EC:DEC (1:1)/Li cells.

amount of hydrogen is sufficient to eliminate this impurity. Hydrogen acts as the reducing agent for iron, preventing the nucleation of the $Li_3Fe_2(PO_4)_3$ phase. With this precaution, $LiFePO_4$ ingots can be obtained in the molten state, free from any impurity. Then, the various stages of grinding and milling make it possible to prepare

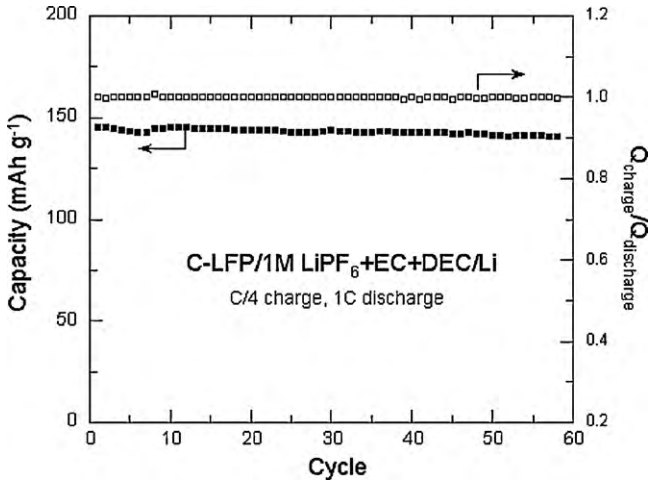

Fig. 17. Cycling of wet-milled C-$LiFePO_4$/1 M $LiPF_6$ + EC:DEC (1:1)/Li cell (discharge rate: 1 C, charge rate C/4) with wet-milled LFP nanoparticles.

$LiFePO_4$ particles of any size, down to the nanometer range. At the last step of the process, the samples prepared in the present work have primary crystalline particles that are approximately spherical with 25 nm average diameter. These particles are slightly agglomerated to form secondary particles of about 100 nm in diameter. The formation of agglomerates of primary particles instead of elementary nanoparticles is beneficial because this facilitate ion and electron diffusion and the electrochemical redox reaction [50]. The nano-dimensions of the active primary particles and the agglomerates of larger size are a desirable combination for electrochemical performance [50].

We learned in our earlier research [47] that, before carbon coating, the surface layer which is a few nanometers thick is strongly disordered, but this disorder is at least partially eliminated by the carbon-coating process. However, we are not certain whether re-crystallization of the surface layer is simply due to heating at 700 °C or if the interaction between carbon and iron plays a major role. The present work shows that there is indeed re-crystallization upon heating at 700 °C because a small but significant improvement of the electrochemical properties is observed by heating at this temperature, even in absence of carbon. On the other hand, good electrochemical properties of the particles are obtained after nanogrinding only with carbon coating, thus confirming definitely our previous claim [47] that a carbon coating is necessary even for nanoparticles. The conclusion that the carbon deposit is not necessary is incorrect. This erroneous conclusion occurred because some authors ignored the fact that some of the carbon in the precursors remained after synthesis [5,6]. Actually, the carbon coating is even more important when the particles are small because more particles per gram are present, so the electric conductivity between particles is enhanced by the carbon, and the performance of the battery is improved.

However, our result is not definitive proof that the carbon itself has an influence in the improvement in crystallinity of the surface layer, although the surface effects plays in favor of such a hypothesis [47]. The reason is that the primary effect of the carbon deposit is to insure electric contact and connectivity between the particles [5–7]. Thus, we cannot conclude that this is the only effect of the carbon layer because heat treatment also affects the surface layer. In any case, the positive result is that the carbon-coated nanoparticles obtained by this process have a high-rate capability up to 30 C.

The major slope in the voltage vs. capacity curve observed in Fig. 13 before carbon coating is in agreement with very similar charge–discharge profiles found for particles with a diameter in the order of 40 nm reported by several authors [58,59]. This behavior is evidence for the reduction of the miscibility by decreasing the particle size to 40 nm. Indeed, according to the Gibbs rule, the voltage plateau is the signature of a two-phase system (Li-rich and Li-poor), while a finite slope indicates a homogeneous phase Li_xFePO_4. Our results, however, contradict this interpretation because the plateau for the carbon-coated particles of even smaller size suggests a different interpretation. The solid solution, as revealed by the slope in the charge–discharge curves for uncoated particles, is located only in the surface layer and not in the "bulk" of the particles. In addition, this solid solution is due to the disorder, since the reduction of the disorder by the carbon-coating process induced a demixing in two phases revealed by the restoration of the plateau. A slope in the charge/discharge profiles was observed [60], however, a very large concentration of defects in the bulk of the particles was detected. This uncontrolled amount of defects is another type of disorder that, in addition to an eventual strong disorder in the surface layer, is responsible for this effect, together with a degradation of the electrochemical performance. One important result of the present work is that the wet-milling process can remove these disorder effects so that the full performance and the electrochemical properties are obtained, just like in bigger particles.

Based on a recent calculation of the electronic structure of $LiFePO_4$ that takes into account the finite size of the particles, a particle diameter of the order of 25 nm is still too large to affect the phase diagram, and the solid solution should still be unstable at room temperature [61]. In this calculation, the surface energy is taken into account, but no disorder is introduced, so that the results should be compared with our experiments for particles after carbon coating. Indeed, our results are in agreement with this calculation, since we find that the charge–discharge profile and the plateau that is the signature of the two-phase system is the same as in the case of bigger particles.

It is difficult to compare the electrochemical performance with prior data published in the literature because the charge rate that is feasible increases with the amount of carbon that is present in the cathode. Tests in the laboratory tend to be performed with larger amounts of carbon to achieve better performance. For instance, with a discharge rate of 20 C, the capacity was 105 mAh g^{-1} and 75 mAh g^{-1} at 60 C [23] with particles that were produced by the wet-milling process [50]. In this example, the cathode contained 70 wt.% $LiFePO_4$ and 20 wt.% acetylene black. An extreme case is 65 wt.% carbon to get ultra high capacity [56], a result that was criticized in [57]. However, in commercial Li-ion batteries, the amount of carbon must be small, usually $\leq$5 wt.%, because carbon is an inert mass. The tests in the present work meet this requirement, as they were performed with 2 wt.% carbon. Nevertheless, the rate capability for the C-$LiFePO_4$ nanoparticles in Li/1 M $LiPF_6$ in EC:DEC (1:1)/C-$LiFePO_4$ is remarkable. Our study demonstrates that nanoparticles prepared from a molten ingot can be used as the active element of the cathode of Li-ion batteries for large-scale applications in plug-in hybrid or fully electric vehicles, after the particles are carbon-coated and heat treated at 700 °C.

5. Conclusion

The results demonstrates that nanoparticles of $LiFePO_4$ prepared by a simple process to form a molten ingot can be used as the active element of the cathode of Li-ion batteries for large-scale applications after the particles have been carbon-coated by heat treatment at 700 °C. In contrast with prior reports, however, carbon coating is mandatory for the nanoparticles. It is actually even more important than for bigger particles because the carbon insures good electrical contact between the particles, and smaller particles require more electrical contacts. The results also reveal that heat treatment at 700 °C is beneficial to improved electrochemical properties, as it induces a re-crystallization that reduces at least partly the structural disorder of the surface layer. Again the nanosize of the particle makes this effect more important because the surface/volume ratio increase compared to bigger particles.

Acknowledgments

The authors are grateful to M. Selmane and F. Gendron for their assistance in XRD and SQUID experiments.

References

[1] A.K. Padhi, K.S. Nanjundswamy, J.B. Goodenough, J. Electrochem. Soc. 144 (1997) 1188.
[2] A.K. Padhi, K.S. Nanjundswamy, C. Masquelier, S. Okada, J.B. Goodenough, J. Electrochem. Soc. 144 (1997) 1609.
[3] K. Zaghib, A. Mauger, J.B. Goodenough, F. Gendron, C.M. Julien, in: J. Garche, C. Dyer, P. Moseley, Z. Ogumi, D. Rand, B. Scrosati (Eds.), Encyclopedia of Electrochemical Power Sources, vol. 5, Elsevier, Amsterdam, 2009, pp. 264–296.
[4] D. Dominko, M. Gaberscek, J. Drofenik, M. Bele, J. Jamnik, Electrochim. Acta 8 (2003) 3709.
[5] N. Ravet, J.B. Goodenough, S. Besner, M. Simoneau, P. Hovington, M. Armand, Proceedings of the 196th ECS Meeting, Honolulu, HI, October, 1999.
[6] N. Ravet, Y. Chouinard, J.F. Magnan, S. Besner, M. Gauthier, M. Armand, J. Power Sources 97 (2001) 503.
[7] S.L. Bewlay, K. Konstantinov, G.X. Wang, S.X. Dou, H.K. Liu, Mater. Lett. 58 (2004) 1788.
[8] Y.D. Cho, G.T.K. Frey, H.-M. Kao, J. Power Sources 189 (2009) 256.
[9] C.-Z. Lu, G.T.K. Frey, H.-M. Kao, J. Power Sources 189 (2009) 155.
[10] K. Zaghib, A. Mauger, F. Gendron, C.M. Julien, Solid State Ionics 179 (2008) 16.
[11] A. Yamasda, S.C. Chung, K. Hinokuma, J. Electrochem. Soc. 148 (2001) A224.
[12] R. Dominko, M. Bele, M. Gaberscek, M. Remskar, D. Hanzel, J.M. Goupil, S. Pejovnik, J. Jamnik, J. Power Sources 153 (2006) 274.
[13] M. Gaberscek, R. Dominko, M. Bele, M. Remskar, D. Hanzel, J. Jamnik, Solid State Ionics 176 (2005) 1801.
[14] S. Yang, P.Y. Zavajil, M.S. Whittingham, Electrochem. Commun. 3 (2001) 505.
[15] J. Chen, M.S. Whittingham, Electrochem. Commun. 8 (2006) 855.
[16] K. Dokko, S. Koizumi, K. Kanamura, Chem. Lett. 35 (2006) 338.
[17] A.V. Murugan, T. Muraliganth, A. Manthiram, J. Electrochem. Soc. 156 (2009) A79.
[18] C. Delacourt, P. Pozot, S. Levasseur, C. Masquelier, Electrochem. Solid State Lett. 9 (2009) A352.
[19] G. Arnold, J. Garche, R. Hemmer, S. Strbele, C. Vogler, M. Wohlfgang-Mehrens, J. Power Sources 119–121 (2003) 247.
[20] H. Kim, J. Kim, Electrochem. Solid State Lett. 9 (2006) A439.
[21] S.T. Myung, S. Komaba, N. Hirosaki, H. Yashiro, N. Kumagai, Electrochim. Acta 49 (2004) 4213.
[22] K. Konstantinov, S. Bewlay, G.X. Wang, M. Lindsay, J.Z. Wang, Electrochim. Acta 50 (2004) 421.
[23] M. Konarova, I. Taniguchi, J. Power Sources 195 (2010) 3661.
[24] Y. Zhang, H. Feng, X. Wu, L. Wang, A. Zhang, T. Xia, H. Dng, M. Liu, Electrochim. Acta 54 (2009) 3206.
[25] I. Bileka, A. Hintennach, I. Djerdj, P. Novak, M. Niederberger, J. Mater. Chem. 19 (2009) 5125.
[26] C.R. Cides, F. Croce, V.Y. Young, C.R. Martin, B. Scrosati, Electrochem. Solid State Lett. 8 (2005) A484.
[27] S. Lim, C.S. Yoon, J. Cho, Chem. Mater. 20 (2008) 4560.
[28] C.M. Doherty, R.A. Caruso, B.M. Smarsly, C.J. Drummond, Chem. Mater. 21 (2009) 2895.
[29] K. Saravanan, M.V. Reddy, P. Balaya, H. Gong, B.V.R. Chowvari, J.J. Vittal, J. Mater. Chem. 19 (2009) 605.
[30] H. Yang, X.-L. Wu, M.-H. Cao, Y.-G. Guo, J. Phys. Chem. C113 (2009) 3345.
[31] B.-J. Hwang, K.-F. Hsu, S.-K. Hu, M.-Y. Cheng, T.-C. Chou, J. Power Sources 194 (2009) 515.
[32] A. Ait-Salah, A. Mauger, C.M. Julien, F. Gendron, Mater. Sci. Eng. B 129 (2006) 232.
[33] D.-H. Kim, Electrochem. Solid State Lett. 9 (2006) A439.
[34] R. Amin, P. Balaya, J. Mayer, Electrochem. Solid State Lett. 10 (2007) A13.
[35] G.X. Wang, S. Bewlay, S.A. Needham, H.K. Liu, R.S. Liu, V.A. Drozd, J.F. Lee, J.M. Chen, J. Electrochem. Soc. 153 (2006) A25.
[36] G. Meligrana, C. Gerbaldi, N. Penazzi, J. Power Sources 160 (2006) 516.
[37] K.F. Hsu, S.Y. Tsay, B.J. Hwang, J. Power Sources 192 (2009) 660.
[38] Z.H. Chen, J.R. Dahn, J. Electrochem. Soc. 149 (2002) A1184.
[39] K. Zaghib, G. Liang, J. Labrecque, A. Mauger, C.M. Julien, Extended Abstract of the 214th ECS Meeting, Honolulu, HI, 2008 (Abs. No. 582).
[40] T. Maxisch, F. Zhou, G. Ceder, Phys. Rev. B 73 (2006) 104301.
[41] M.S. Islam, D.J. Driscoll, C.A. Fischer, P.R. Slater, Chem. Mater. 17 (2005) 5085.
[42] G. Chen, X. Song, T.J. Richardson, J. Electrochem. Soc. 154 (2007) A627.
[43] T.J. Richardson, 3rd Annual Conference—Lithium Mobile Power 2007—Advances in Lithium Battery Technologies for Mobile Applications, San Diego, CA, 2007.
[44] G. Chen, X. Song, T.J. Richardson, J. Electrochem. Solid State Lett. 9 (2006) A295.
[45] L. Laffont, C. Delacourt, P. Gibot, M. Yue Wu, P. Kooyman, C. Masquelier, J.M. Tarascon, Chem. Mater. 18 (2006) 5520.
[46] K. Dokko, S. Koizumi, H. Nakano, K. Kanamura, J. Mater. Chem. 17 (2007) 4803.
[47] K. Zaghib, A. Mauger, F. Gendron, C.M. Julien, Chem. Mater. 20 (2008) 462.
[48] L. Gauthier, M. Gauthier, D. Lavoie, C. Michot, N. Ravet, US Patent 7,534,408 B2.
[49] P. Axmann, C. Stinner, M. Wohlfahrt-Mehrens, A. Mauger, F. Gendron, C.M. Julien, Chem. Mater. 21 (2009) 1636.
[50] G. Luang, P. Charest, C. Michot, A. Guerfi, M. Gauthier, K. Zaghib, Patent WO 2008/0676677 A1.
[51] N. Ravet, M. Gauthier, K. Zaghib, A. Mauger, J. Goodenough, F. Gendron, C.M. Julien, Chem. Mater. 19 (2007) 2595.
[52] C.M. Julien, K. Zaghib, A. Mauger, M. Massot, M. Ait-Salah, F. Selmane, Gendron, J. Appl. Phys. 100 (2006) 63511.
[53] M.T. Paques-Ledent, P. Tarte, Spectrochim. Acta A30 (1974) 673.
[54] P. Jozwiak, J. Garbarczik, F. Gendron, A. Mauger, C.M. Julien, J. Non-Cryst. Solids 354 (2008) 1915.
[55] R.M. Garberscek, R. Dominko, J. Jamnik, Electrochem. Commun. 9 (2008) 2778.
[56] B. Kang, G. Ceder, Nature 458 (2009) 190.
[57] K. Zaghib, J.B. Goodenough, A. Mauger, C. Julien, J. Power Sources 194 (2009) 1021.
[58] N. Meetong, H. Huang, W.C. Carter, Y.M. Chiang, Electrochem. Solid State Lett. 10 (2007) A134.
[59] G. Kobayashi, S. Nishimura, M. Park, R. Kanno, M. Yashima, T. Ida, A. Yamada, Extended Abstract of the 214th ECS Meeting, Honolulu, HI, 2008 (Abs. No. 628).
[60] P. Gibot, M. Casas-Cabanas, L. Laffont, S. Levasseur, P. Carlach, S. Hamelet, J.-M. Tarascon, C. Masquelier, Nat. Mater. 7 (2008) 741.
[61] G. Ceder, L. Wang, A. Belcher, Y. Lee, K. Kang, Extended Abstract of the 214th ECS Meeting, Honolulu, HI, 2008 (Abs. No. 627).